European Laboratory for Particle Physics

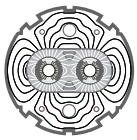

Large Hadron Collider Project

LHC Project Report 199

Energy lost by a particle beam in a lossy coaxial liner with many holes

Andrea Mostacci

Abstract

In the framework of Bethe's modified theory we study the energy lost by a relativistic particle beam travelling in a coaxial liner with many holes, including the effect of attenuation in the coaxial region. The interference among the holes is the main source of losses and is affected by the attenuation in the coaxial only on sufficiently long distances. We derive analytical formulae for all the interesting quantities and a particular attention is given in clarifying the physical meaning; numerical examples are considered using the LHC nominal parameters.

Administrative Secretariat
LHC Division
CERN
CH-1211 Geneva 23
Switzerland

Geneva, 3 July 1998

1 Introduction

Several papers have been devoted to the interaction between a particle beam and the pumping holes, usually described in terms of coupling impedance and loss factor. In particular we are interested in the structure sketched in Fig. 1: the holes couple the vacuum chamber (a circular wave-guide) to the external ante-chamber (a coaxial wave-guide).

The problem has been solved by means of the modified Bethe's diffraction theory for a single hole in [1] and for N holes in [2], if they are small with respect to the wavelength λ. Recently this theory has been further modified to estimate analytically the effects of a long narrow slot [3]. Some measurements were also performed on a LHC vacuum chamber prototype [4] (i.e. coaxial chamber with many holes) to estimate the power lost by the beam because of these holes and the results were explained with a simplified model. The original Bethe's diffraction theory [5] has been used to study the effect of a single hole [6] in the beam pipe as well as many holes [7], for a pipe wall of infinite thickness so that there is no coupling with any external structure. Other techniques often used are the field matching method [8] and a variational approach [9].

In this paper we review previous results in the case of many holes, but including also the effect of field attenuation in the coaxial region. This case has not yet been studied in the framework of the modified Bethe theory and it is interesting in the project of future machines such as LHC. A possible attenuation source is the ohmic loss in the walls of the coaxial, but some other could be foreseen as well (as for instance proper attenuators). We will focus mainly on the first case, but our theory can be easily extended to other ones.

The modified Bethe's theory states that each hole is equivalent to magnetic and electric dipoles whose moments are proportional through appropriate hole polarizabilities to the fields propagating both in the beam pipe and in the coaxial region.

We consider a single relativistic charge travelling along the z-axis and start by studying the problem in a frequency range below all possible cut-offs, i.e. including only the TEM field propagating in the coaxial. Its amplitude depends on the dipole moments (that are the source of that field); we can derive a linear inhomogeneous system whose unknowns are the dipole moments and whose forcing term is the field of the charge. Once the system has been solved, we can express the field in each point of the structure in terms of the dipole moments; in particular we can compute the z-component of the electric field on the axis and then the longitudinal coupling impedance [10]. The loss factor follows easily: for example with a Gaussian bunch we can apply Eq. (39) in the case of N holes obtaining Eq. (40). The results are in good agreement with MAFIA simulations [1, 2].

A further extension in frequency is possible including more modes, both in the circular and in the coaxial waveguide, although this is not necessary for long bunches (as in hadron machines), since the frequencies excited are usually below all possible cut-offs.

This paper is organised as follows: we first study the ideal structure of a pipe with thin wall ($b_1 = b_2 = b$), then we briefly discuss the effect of wall thickness, how it can be taken into account and we make some comparisons with existing estimates.

In Sec. 2 a formula for the coupling impedance valid for any spacing between the holes and for any attenuation source in the coaxial is derived. Since it has been demonstrated [2] that the loss factor is not considerably influenced by the randomisation of the position of the holes, we focus on equally spaced holes (one hole per cross section): the goal is to give and discuss simplified formulae useful for the following calculations. Sec. 3 applies those results to the loss factor: we arrive at an analytical formula both when there are no losses in the coaxial and when we treat the ohmic ones. Still in the ideal case of thin wall, we discuss in Sec. 4 the power lost per unit length in the coaxial region. We also

recall how to account for many holes on a cross section. Sec. 5 specifies how to modify the previous results for holes in a thick wall. A comparison with [4] is done in Sec. 6, confirming our results. Throughout the paper, all the examples are done using LHC nominal parameters; in Sec. 7 we summarise the results most relevant for the project.

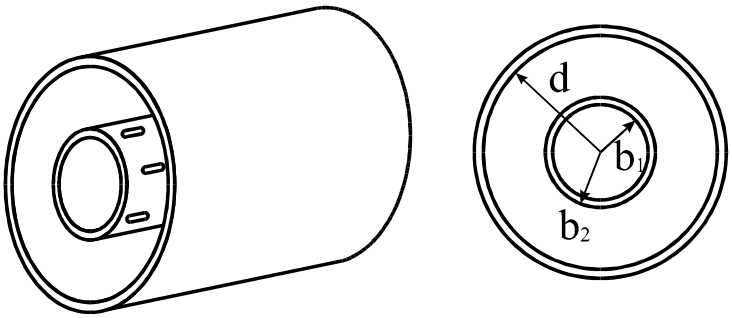

Figure 1: Relevant geometries

Caption	Symbol	Numerical Value
wave number	$k_0 = \omega/c$	
attenuation constant[1)]	$\alpha(\omega) = a\sqrt{\omega}$	
device length	L_d	14 m $\div$ 27 km
number of holes	N	870 $\div$ 1.7 10^6
number of holes per cross section	N_b	1$\div$8
bunch charge	Q	16 nC
bunch length	σ	7.5 cm
bunch cut-off	f_c	640 MHz
bunch spacing	S_b	7.5 m
coaxial walls resistivity (stainless steel)	ρ	7.1×10^{-7} Ωm
inner pipe radius	b_1	1.9 cm
outer pipe radius	$b_2 = b_1 + T$	2 cm
cold bore radius	d	2.45 cm
wall thickness	T	1 mm
hole spacing	D	1.6 cm
hole width	W	1.5 mm
hole length	L	8 mm
radius of circular holes	$R = W/2$	0.75 mm

Table 1: List of symbols used throughout the paper. Plots and examples refer to the LHC numerical values reported in the third column, unless otherwise specified.

1.1 Outline of the general theory

The general theory adopted in these calculations is described in [1, 2]; for convenience, we summarise its main features at frequencies below the beam pipe cut-off considering only scattered TEM-type fields, in the case of N holes.

[1)] This behaviour of α with the frequency is only valid for non-anomalous ohmic losses; we report it in this table only for reader's convenience.

We will use cylindrical coordinates, with z being the longitudinal coordinate, r and φ the radial and the azimuthal ones. The subscript "0" on a field means that it is a source field (charge field), while the fields with subscript "s" are the scattered ones propagating in coaxial region.

Bethe's diffraction theory [12] states that each hole is equivalent to an electric and a magnetic dipole whose moments are given by

$$\begin{aligned} M_\varphi(z_i) &= \alpha_m \left[H_{0\varphi}(z_i) - H_{s\varphi}(z_i)\right], \\ P_r(z_i) &= \varepsilon\alpha_e \left[E_{0r}(z_i) - E_{sr}(z_i)\right], \end{aligned} \qquad i = 1, \ldots, N \tag{1}$$

where α_m and α_e are the polarizabilities of the hole and $H_{s\varphi}$, E_{sr} is the scattered field calculated at the centre of the hole with longitudinal coordinate z_i. The primary field, generated by an ultra-relativistic point charge q, travelling along the axis of a perfectly conducting beam pipe of radius b, is ($k_0 = \omega/c$)

$$H_{0\varphi}(z_i) = \frac{q}{2\pi b} e^{-jk_0 z_i}, \; E_{0r}(z_i) = Z_0 \frac{q}{2\pi b} e^{-jk_0 z_i} \tag{2}$$

In [2], the TEM-type scattered fields are supposed to have the same phase velocity as the charge. We remove this hypothesis allowing for a complex propagation constant of the form

$$k_c = k_0 - j\alpha, \tag{3}$$

where α is the attenuation constant. Both k_0 and α are given functions of the frequency ω with dimensions of $[\mathrm{m}^{-1}]$. If the attenuation constant is a real quantity, the field will be exponentially damped along the propagation direction (z-axis); the source of this attenuation fixes the ω-dependence of α. On the other hand, a purely imaginary α takes into account a slowing down of the TEM fields in the external coaxial region; that could be, for example, the effect of a long series of uniformly spaced holes acting as the periodic perturbation of boundary conditions in any slow-wave device.

In general the scattered fields can be expressed as a superposition of modes. The coefficients of the modal expansion are determined through the Lorentz reciprocity principle [12]; they are linear functions of the equivalent dipole moments of the apertures which can be obtained solving a $2N \times 2N$ linear system.

Once the equivalent dipole moments have been determined, we can calculate the longitudinal coupling impedance, using the result [2]

$$Z(\omega) = j\frac{\omega Z_0}{2\pi q b} \sum_{i=1}^{N} \left[\frac{M_\varphi(z_i)}{c} + P_r(z_i)\right] e^{jk_0 z_i} \tag{4}$$

The longitudinal coupling impedance is the Green function of the problem; the loss factor depends on its real part, since [10]

$$k(\sigma) = \frac{1}{\pi} \int_0^\infty Z_{RE}(\omega)\, e^{-\left(\frac{\omega\sigma}{c}\right)^2} d\omega,$$

for a Gaussian bunch of length σ.

The previous quantities are important for the LHC beam dynamics. On the other hand, since the bunch will excite the TEM mode in the coaxial region, this will dissipate some power on the walls of the coaxial (stainless steel) causing heating of the cold bore.

This is an essential parameter in the project of the machine; to estimate it, we introduce the dissipated power per unit length P, expressed in terms of the loss factor as

$$P = \frac{c\, Q^2\, k\,(\sigma)}{S_b\, L_d},$$

where Q is the bunch charge, S_b the bunch separation, L_d the device length and $k\,(\sigma)$ is the loss factor due to the N holes in the device.

2 Longitudinal coupling impedance

Each hole in the beam pipe is a source of electromagnetic field propagating in the coaxial region and can be characterised by equivalent dipole moments (electric and magnetic); Eq. (4) gives the longitudinal coupling impedance in terms of these moments. Here we derive analytical results for the coupling impedance when an attenuation source is present in the coaxial region; the numerical examples we give, are all done using LHC nominal parameters and the attenuation source is the ohmic loss on the walls of the coaxial region (see Fig. 1).

Having derived the coupling impedance for general spacing between the holes (Sec. 2.1), we then specify our treatment to uniformly spaced holes (Sec. 2.2). In the latter case, we give and comment a general formula focusing on the physical meaning of each term and showing the importance of the interference effects due to the TEM mode propagating in the coaxial structure; an approximate formula (valid in the nominal case of LHC) is also derived and discussed. In Sec. 2.3 we make remarks on the effect of the TEM field propagating in the same direction of the bunch, comparing with the complete case (i.e. including also the field propagating in the opposite direction).

2.1 General derivation

2.1.1 From dipole moments ...

The dipole moments obey a linear system whose forcing term depends on the field of the bunch over each hole. After having derived formally this system, we obtain a first order solution: we first give an analytical expression for M_φ and P_r, then we check their agreement with the already studied case of no attenuation in the coaxial; eventually we try to clarify the physical meaning of each term of the dipole moments formula.

To find the expression for the dipole moments on each hole, we replace in their definition (Eqs. (1)) the scattered field. A TEM field radiated by a hole centred in $z = z_i$ can be written as

$$\begin{aligned} E_{sr}\,(z, z_i) &= c_{0i} e_{0r} e^{-jk_c(z-z_i)} \theta\,(z - z_i) + d_{0i} e_{0r} e^{jk_c(z-z_i)} \theta\,(-z + z_i) \\ H_{s\varphi}\,(z, z_i) &= c_{0i} h_{0\varphi} e^{-jk_c(z-z_i)} \theta\,(z - z_i) - d_{0i} h_{0\varphi} e^{jk_c(z-z_i)} \theta\,(-z + z_i)\,, \end{aligned} \tag{5}$$

where k_c is the propagation constant, $\theta(z)$ the Heaviside function

$$\theta(z) = \begin{cases} 1 & \text{for } z > 0 \\ 0 & \text{for } z < 0 \end{cases}$$

and $e_{0r}, h_{0\varphi}$ are the normalised modal functions for the TEM mode

$$e_{0r} = \sqrt{\frac{Z_0}{2\pi}}\, \frac{1}{\sqrt{\ln\,(d/b)}}\, \frac{1}{r}, \quad h_{0\varphi} = \frac{1}{Z_0} e_{0r}. \tag{6}$$

The coefficients c_{0i} and d_{0i} depend on the source field and they are

$$c_{0i} = \frac{j\omega}{2}\left[\mu h_{0\varphi} M_\varphi(z_i) + e_{0r} P_r(z_i)\right]$$
$$d_{0i} = -\frac{j\omega}{2}\left[\mu h_{0\varphi} M_\varphi(z_i) - e_{0r} P_r(z_i)\right], \tag{7}$$

according to Lorentz reciprocity principle (see for instance [2]). The scattered field $E_{sr}, H_{s\varphi}$ in a generic hole, centred in z_i, appearing in Eq. (1) is the sum of the field scattered by each hole, thus

$$E_{sr}(z_i) = e_{0r}\left[\sum_{k=1}^{i-1} c_{0k} e^{-jk_c(z_i - z_k)} + \frac{c_{0i} + d_{0i}}{2} + \sum_{k=i+1}^{N} d_{0k} e^{jk_c(z_i - z_k)}\right],$$
$$H_{s\varphi}(z_i) = h_{0\varphi}\left[\sum_{k=1}^{i-1} c_{0k} e^{-jk_c(z_i - z_k)} + \frac{c_{0i} + d_{0i}}{2} - \sum_{k=i+1}^{N} d_{0k} e^{jk_c(z_i - z_k)}\right]; \tag{8}$$

it depends, through c_{0i} and d_{0i}, on the dipole moments themselves. Replacing Eq. (7) in Eq. (8) one obtains

$$M_\varphi(z_i) = \alpha_m\left[H_{0\varphi}(z_i) - j\frac{\omega}{2}\mu h_{0\varphi}^2 \sum_{h=1}^{N} M_\varphi(z_h) e^{-jk_c|z_h - z_i|} + \right.$$
$$\left. + j\frac{\omega}{2} h_{0\varphi} e_{0r} \sum_{h=1}^{N} P_r(z_h) sgn(h-i) e^{-jk_c|z_h - z_i|}\right]$$
$$P_r(z_i) = \varepsilon\alpha_e\left[E_{0r}(z_i) - j\frac{\omega}{2} e_{0r}^2 \sum_{h=1}^{N} P_r(z_h) e^{-jk_c|z_h - z_i|} + \right.$$
$$\left. + j\frac{\omega}{2}\mu h_{0\varphi} e_{0r} \sum_{h=1}^{N} M_\varphi(z_h) sgn(h-i) e^{-jk_c|z_h - z_i|}\right]. \tag{9}$$

Eqs. (9) are an inhomogeneous $2N \times 2N$ linear system whose unknowns are the dipole moments M_φ and P_r. Using the first order iterative solution discussed in [2], i.e. substituting in the right-hand side of Eqs. (9) the approximate values (that is the zero order solution)

$$M_\varphi^{(0)}(z) = \alpha_m H_{0\varphi}(z) \quad \text{and} \quad P_r^{(0)}(z) = \varepsilon\alpha_e E_{0r}(z), \tag{10}$$

we get (see Appendix A)

$$M_\varphi(z_i) \simeq \alpha_m H_{0\varphi}(z_i)\left\{1 - j\frac{k_0}{4\pi b^2 \ln(d/b)}\left[\alpha_m + (\alpha_e + \alpha_m) F_i\, e^{-\alpha z_i} + (\alpha_m - \alpha_e) B_i\right]\right\},$$
$$P_r(z_i) \simeq \varepsilon\alpha_e E_r(z_i)\left\{1 - j\frac{k_0}{4\pi b^2 \ln(d/b)}\left[\alpha_e + (\alpha_e + \alpha_m) F_i\, e^{-\alpha z_i} - (\alpha_m - \alpha_e) B_i\right]\right\}, \tag{11}$$

where

$$F_k = \sum_{w=1}^{k-1} e^{\alpha z_w} \quad \text{and} \quad B_k = \sum_{w=1}^{N-k} e^{-(j2k_0 + \alpha)(z_{w+k} - z_k)}.$$

We remind that each hole is identified by the position of its centre (z_k) with respect to the first hole ($z_1 = 0$). In spite of their apparent complexity, Eqs. (11) allow us to treat directly any kind of spacing between the holes.

In the limit of low attenuation ($\alpha(\omega)\, z_k \to 0 \quad \forall\, \omega$ and $k = 1, \ldots, N$), we find that

$$F_k \to k-1 \quad \text{and} \quad B_k = \sum_{w=1}^{N-k} e^{-j2k_0(z_{w+k}-z_k)}, \tag{12}$$

leading to the results already given in [2].

Before going on, we may clarify the physics behind Eqs. (11). Rewriting only the equation for $M_\varphi(z_h)$ with no attenuation, yields

$$M_\varphi(z_h) \simeq \alpha_m H_{0\varphi}(z_h) \left\{ 1 - j\frac{k_0}{4\pi b^2 \ln(d/b)} \left[\alpha_m + (\alpha_e + \alpha_m)(h-1) + \right.\right.$$
$$\left.\left. + (\alpha_m - \alpha_e) \sum_{w=1}^{N-h} e^{-j2k_0(z_{w+h}-z_h)} \right] \right\}. \tag{13}$$

In the square brackets we recognise three terms, with the following meaning:

term $\propto \alpha_m$**:** it is the effect of the hole on itself and it is present even with a single hole ($h = N = 1$).

term $\propto (\alpha_m + \alpha_e)$**:** it is the effect of the preceding holes; the h-th hole has $h-1$ preceding holes which are interacting with it by means of a forward propagating TEM wave. Since the charge field and the TEM wave are synchronous, there is no phase factor in this term.

term $\propto (\alpha_m - \alpha_e)$**:** this is the effect of the following holes interacting with the h-th hole through the backward propagating TEM wave. Since charge field and the TEM wave have the same phase velocity but they are going in opposite direction, the phase factor turns out to be twice the phase shift due to propagation from the hole in z_{w+h} to the one in z_h.

The distinction between "following" and "preceding" holes doesn't contradict the causality principle since we are reasoning in the fictitious Fourier space, that is considering sine waves going from time $t = +\infty$ to $t = -\infty$ at frequency ω. Moreover we notice that the forward and the backward propagating waves have different weights depending on the values of the polarizabilities (α_m, α_e have opposite signs). For circular holes $|\alpha_m|$ and $|\alpha_e|$ are different by a factor 2, while for long slots they can be very similar (slot length much larger than its width). Thus we expect that for rounded-end slots the contribution of backward propagating waves is more relevant than for circular holes. We will use this fact later. The same reasoning can be performed for $P_r(z_i)$; attenuation doesn't change substantially those arguments.

2.1.2 ... to impedance.

We now use the previous results for the dipole moments to find the coupling impedance as a function of the position of each hole. Eventually we briefly discuss the limit of very low and very high attenuation.

Using the expressions (11) in Eqs. (4), we obtain the following relations for the imaginary part Z_{IM} and the real part Z_{RE} of the longitudinal coupling impedance the following relations

$$Z_{IM}(\omega) = Z_0 \frac{\omega}{4\pi^2 b^2 c} \left\{ N(\alpha_m + \alpha_e) + \right.$$
$$\left. - \frac{\omega}{4\pi b^2 \ln(d/b) c} (\alpha_m - \alpha_e)^2 \sum_{h=1}^{N-1} \sum_{w=1}^{N-h} e^{-\alpha(z_{w+h}-z_h)} \sin\left[2\frac{\omega}{c}(z_{w+h} - z_h) \right] \right\} \tag{14}$$

and

$$Z_{RE}(\omega) = Z_0 \frac{\omega^2}{16\pi^3 b^4 \ln(d/b) c^2} \left\{ N\left(\alpha_m^2 + \alpha_e^2\right) + (\alpha_m + \alpha_e)^2 \sum_{h=1}^{N} F_h e^{-\alpha z_h} + \right.$$
$$\left. + (\alpha_m - \alpha_e)^2 \sum_{h=1}^{N-1} \sum_{w=1}^{N-h} e^{-\alpha(z_{w+h} - z_h)} \cos\left[2\frac{\omega}{c}(z_{w+h} - z_h)\right] \right\}. \qquad (15)$$

It is worth noting that Z_{IM} has a dominant term independent of the position of the holes and equal to N times the impedance of a single hole. The attenuation doesn't play an important role in this case. Its effect is more remarkable on the real part Z_{RE} since the latter strongly depends on the spacing among the holes, as already shown in [2].

In the limit of low attenuation ($\alpha(\omega)\, z_k \to 0 \quad \forall\, \omega$ and $k = 1, \ldots, N$),

$$\sum_{h=1}^{N} F_h e^{-\alpha z_h} \to \frac{N}{2}(N-1) \quad \text{and} \quad \sum_{h=1}^{N} B_h \to \sum_{h=1}^{N-1} \sum_{w=1}^{N-h} e^{-j2k_0(z_{w+h} - z_h)}; \qquad (16)$$

those lead to the known expression for the coupling impedance when there are no losses in the coaxial region [2].

On the contrary, if the losses are such that the field scattered by one hole doesn't reach the others (namely $\alpha(\omega) \to \infty$) there is no effective interference between them and we expect also the real part of the impedance to be N times the impedance of a single hole; in this limit, indeed,

$$Z_{RE}(\omega) \to Z_0 \frac{\omega^2}{16\pi^3 b^4 \ln(d/b) c^2} N\left(\alpha_m^2 + \alpha_e^2\right). \qquad (17)$$

Thus, increasing the attenuation in the coaxial reduces the coupling impedance until this last term becomes dominating.

2.2 Uniformly spaced holes

We now deal with uniformly spaced holes; after having derived the complete expression for the longitudinal coupling impedance, we will discuss some simplifications in order to arrive to a more clear and easy-to-treat formula and then we conclude by introducing approximations useful in the following analytical studies of loss factor and power loss per unit length.

Denoting by D the (uniform) distance between two consecutive holes,

$$z_h = (h-1)D \quad \text{and} \quad z_{w+h} - z_h = wD;$$

we can rewrite Eq. (15) as

$$Z_{RE}(\omega) = Z_0 \frac{\omega^2}{16\pi^3 b^4 \ln(d/b) c^2} \left[N\left(\alpha_m^2 + \alpha_e^2\right) + \right.$$
$$\left. + (\alpha_m + \alpha_e)^2 F(D, N, \alpha) + (\alpha_m - \alpha_e)^2 B(D, N, \alpha, \omega) \right] \qquad (18)$$

where

$$F(D, N, \alpha) = \sum_{h=1}^{N} \sum_{k=1}^{h-1} e^{\alpha(z_k - z_h)} = \sum_{h=1}^{N} \sum_{k=1}^{h-1} e^{\alpha(k-h)D} \qquad (19)$$

and

$$B\left(D,N,\alpha,\omega\right)=\sum_{h=1}^{N-1}(N-h)e^{-\alpha hD}\cos\left(2h\frac{\omega}{c}D\right). \tag{20}$$

It is again straightforward to give to those terms their physical meaning: the first one ($\propto N\left(\alpha_m^2+\alpha_e^2\right)$) is the contribution of non interacting holes, while the term weighted by $F\left(D,N,\alpha\right)$ ($B\left(D,N,\alpha,\omega\right)$) is due to the forward (backward) propagating TEM wave.

In the limit of low attenuation ($\alpha DN\to 0$),

$$F\left(D,N,\alpha\right)\to\frac{N}{2}(N-1)\quad\text{and}\quad B\left(D,N,\alpha,\omega\right)\to\frac{1}{2}\left[\frac{\sin\left(N\omega D/c\right)}{\sin\left(\omega D/c\right)}\right]^2-\frac{N}{2};$$

the latter is obtained from the limit of Eq. (20) using the following Eq. (25). Thus inserting those in Eq. (18), we find for the coupling impedance

$$Z_{RE}(\omega)=Z_0\frac{\omega^2}{32\pi^3b^4\ln\left(d/b\right)c^2}\left\{N^2\left(\alpha_m+\alpha_e\right)^2+\left(\alpha_m-\alpha_e\right)^2\left[\frac{\sin\left(N\omega D/c\right)}{\sin\left(\omega D/c\right)}\right]^2\right\}, \tag{21}$$

as already reported in [2].

We now give explicit expressions for Eqs. (19-20) (Sec. 2.2.1 - 2.2.2) and then look for an approximate coupling impedance (Sec. 2.2.3).

2.2.1 Simplification of the term accounting for forward waves

Performing the sums that define $F(D,N,\alpha)$, we get

$$F(D,N,\alpha)=\frac{\left(e^{-\alpha DN}-1\right)e^{\alpha D}+N\left(e^{\alpha D}-1\right)}{\left(e^{\alpha D}-1\right)^2}. \tag{22}$$

As we would expect, when $\alpha D\to\infty$, $F(D,N,\alpha)\to 0$, while in the limit of low attenuation we find, coherently with Eq. (16),

$$F(D,N,\alpha)\to\frac{N}{2}(N-1)\quad\text{for}\quad\alpha DN\to 0. \tag{23}$$

If the spacing of the pumping holes is small compared to the inverse of the attenuation constant (namely $\alpha D\ll 1$), Eq. (22) yields

$$F(D,N,\alpha)\simeq\frac{N}{\alpha D}+\frac{e^{-\alpha DN}-1}{(\alpha D)^2}; \tag{24}$$

this is the case, for instance, of the LHC in which that relation holds for all the frequencies in the bunch spectrum. Anyway we should notice that Eq. (23) is not exactly fulfilled since

$$\frac{N}{\alpha D}+\frac{e^{-\alpha DN}-1}{(\alpha D)^2}\to\frac{N}{2}\quad\text{for}\quad\alpha D\to 0;$$

nevertheless since we are usually dealing with a large number of holes ($N\gg 1$), the error introduced using Eq. (24) is negligible.

2.2.2 Simplification of the term accounting for backward waves

$$B\left(D,N,\alpha,k_0\right)=\sum_{h=1}^{N-1}(N-h)e^{-\alpha Dh}\cos\left(2hk_0D\right),\quad\text{with}\quad k_0=\frac{\omega}{c}.$$

The direct numeric evaluation of this term is very time consuming, at least for the numbers N of interest (for the 14 m long LHC dipole, N is around 900). We now present two different methods to set a more easy-to-treat expression giving complementary results.

Before going through the first derivation, we recall the following relations:

$$\sum_{h=1}^{N-1}(N-h)\cos\left(2hx\right)=\frac{1}{2}\left[\frac{\sin^2\left(Nx\right)}{\sin^2 x}-N\right], \tag{25}$$

$$\sum_{h=1}^{N-1}(N-h)\sin\left(2hx\right)=\frac{N\sin\left(2x\right)-\sin\left(2Nx\right)}{4\sin^2 x}. \tag{26}$$

Expanding the exponential as a sum of complex sine and cosine leads to

$$B=\sum_{h=1}^{N-1}(N-h)\left[\cos\left(j\alpha Dh\right)+j\sin\left(j\alpha Dh\right)\right]\cos\left(2hk_0D\right), \tag{27}$$

or equivalently to

$$\begin{aligned}B=&\frac{1}{2}\sum_{h=1}^{N-1}(N-h)\cos\left(2h\gamma^+D\right)+\frac{1}{2}\sum_{h=1}^{N-1}(N-h)\cos\left(2h\gamma^-D\right)+\\&+\frac{j}{2}\sum_{h=1}^{N-1}(N-h)\sin\left(2h\gamma^+D\right)-\frac{j}{2}\sum_{h=1}^{N-1}(N-h)\sin\left(2h\gamma^-D\right),\end{aligned} \tag{28}$$

where $\gamma^{\pm}=k_0\pm j\alpha/2$. Thus, inserting Eqs. (25–26), we get

$$\begin{aligned}B=&\frac{1}{4}\left[\frac{\sin^2\left(N\gamma^+D\right)}{\sin^2\left(\gamma^+D\right)}-N\right]+\frac{1}{4}\left[\frac{\sin^2\left(N\gamma^-D\right)}{\sin^2\left(\gamma^-D\right)}-N\right]+\\&+\frac{j}{2}\frac{N\sin\left(2\gamma^+D\right)-\sin\left(2N\gamma^+D\right)}{4\sin^2\left(\gamma^+D\right)}-\frac{j}{2}\frac{N\sin\left(2\gamma^-D\right)-\sin\left(2N\gamma^-D\right)}{4\sin^2\left(\gamma^-D\right)}.\end{aligned} \tag{29}$$

To better understand each term of this last equation, we can rewrite it as

$$\begin{aligned}B=&-\frac{N}{2}+j\frac{N}{4}\left[\cot\left(\gamma^+D\right)-\cot\left(\gamma^-D\right)\right]+\\&+\frac{1}{8}\left[\frac{2\sin^2\left(N\gamma^+D\right)-j\sin\left(2N\gamma^+D\right)}{\sin^2\left(\gamma^+D\right)}+\frac{2\sin^2\left(N\gamma^-D\right)+j\sin\left(2N\gamma^-D\right)}{\sin^2\left(\gamma^-D\right)}\right].\end{aligned} \tag{30}$$

Fig. 2 is a plot of B as a function of frequency, using the LHC nominal parameters (see [17]); the attenuation constant α is chosen to depend on the square root of the frequency (case of non anomalous ohmic losses in the coaxial region). The constant term $-N/2$ in Eq. (30) gives the minimum value of the plateau; the second term is (roughly speaking) responsible for the main peaks. They occur at frequencies such that

$$k_0D=n\pi\quad\text{that is}\quad f_n=n\frac{c}{2D}; \tag{31}$$

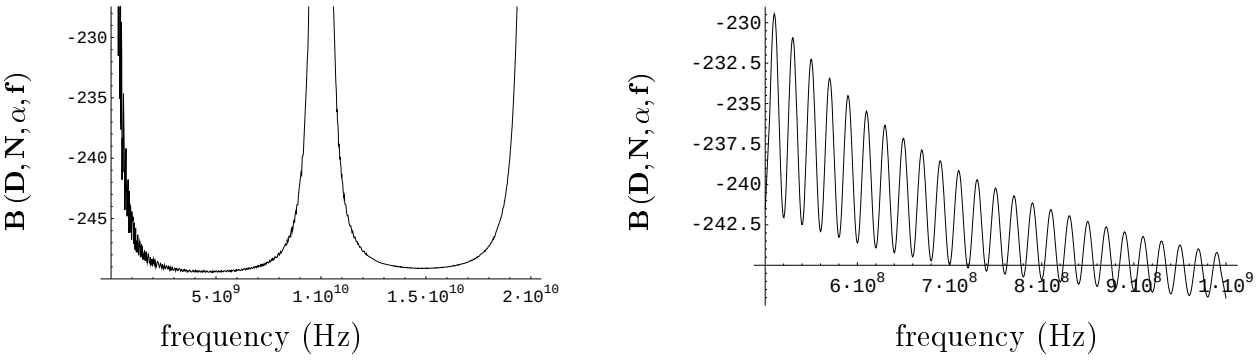

a) **b)**

Figure 2: The coefficient $B(D, N, \alpha, f)$ as a function of frequency (Hz) for $N = 500$ holes. The attenuation constant α depends on the square root of the frequency (see Eq. (45)); all the parameters are chosen as in the case of LHC (see Table 1). (b) is a zoom of the "plateau" between the peaks and shows the presence of a ripple. Since α is increasing with frequency ($\alpha \propto \sqrt{\omega}$), the attenuation is more efficient at higher frequencies and thus the ripple becomes smaller. For lower N, the amplitude of the ripple increases.

their width depends on the attenuation constant and their height is proportional to N^2. Due to the small value of D those frequencies are well above the relevant part of the bunch spectrum; infact if we assume a longitudinal Gaussian beam with r.m.s. bunch length σ, its frequency spectrum is still Gaussian with a r.m.s. frequency of $f_c = c/2\pi\sigma$ (at top energy, $\sigma = 7.5\,\mathrm{cm}$ implies $f_c = 640\,\mathrm{MHz}$); f_c is sometimes called cut-off frequency of the bunch. The planned partial randomisation of the position of the holes widens those peaks and reduces their heights even if it doesn't affect the loss factor (see [2]). Moreover we just have to mention that at those frequencies other modes are propagating both in the coaxial region and in the beam pipe and they are no longer synchronous with the beam. Due to imperfections in the coaxial region (the holes themselves or anything perturbing our ideal geometry), they can exchange energy with the TEM mode we are treating and therefore this scenario could be too pessimistic. Anyway, a detailed study in this sense has not been done, at least for many holes; for a single hole a numerical study based on field matching method has been performed (see [8]) and the results agree with what reported here. As shown in Fig. 2, there is a ripple superimposed onto the plateau; as it can be seen from the third term in Eq. (30), its frequency is

$$N k_0 D = \pi \quad \text{that is} \quad f = \frac{c}{2DN}. \tag{32}$$

Strictly speaking, the third term in Eq. (30) gives also a minor contribution to the values of the peaks. Increasing the amount of attenuation the peaks widen and their height decreases, while the frequency of the ripple and the minimum value of the plateau remain unchanged; a deeper study of Eq. (30) can help in giving a quantitative evaluation of this effects.

It is worth remarking that B (i.e. the effect of backward propagating waves) has a component not depending on the frequency (nor on the attenuation). So even if the major peaks are surely out of the bunch spectrum, the backward propagating wave has indeed an effect at low frequency.

An automatic evaluation of B, based on Eq. (30) is still very time consuming, so

we propose to simplify it by rewriting the cosine in B as the real part of a complex exponential so that

$$B = Re\left[\sum_{h=1}^{N-1}(N-h)e^{-\alpha Dh - j2hk_0D}\right] = Re\left[\sum_{h=1}^{N-1}(N-h)e^{-\beta Dh}\right] \quad \text{with} \quad \beta = \alpha + j2k_0. \tag{33}$$

It is easy to see that

$$\sum_{h=1}^{N-1}(N-h)q^h = \frac{q\left(N - Nq + q^N - 1\right)}{(1-q)^2}; \tag{34}$$

using this relation with $q = e^{-\beta D}$ and taking the real part we obtain the exact value for B. We have used it in drawing Fig. 2 and we will use it in all the following numerical calculations.

Far away from the resonances and for large numbers N, we can approximate B simply with the constant value of Eq. (30); we will exploit this later, since the peak at low frequency has no big effect on the overall impedance because the contribution due to B is weighted by the frequency squared. What is lost in this approximation is the contribution of the ripple, but the latter becomes more and more negligible with increasing number of holes.

2.2.3 An approximate expression for the coupling impedance

We already discussed useful approximations for $F(D, N, \alpha)$ and $B(D, N, \alpha)$; our aim is now to put them together in a simplified expression for the coupling impedance. This will be important later for the analytical estimate of the loss factor.

Recalling that

$$F(D, N, \alpha) \simeq \frac{N}{\alpha D} + \frac{e^{-\alpha DN} - 1}{(\alpha D)^2} \quad \text{for} \quad \alpha D \ll 1,$$

$$B(D, N, \alpha, \omega) \simeq -\frac{N}{2} \quad \text{far from the peaks}$$

and inserting in Eq. (18) yields

$$Z_{RE}(\omega) \simeq Z_0 \frac{\omega^2 (\alpha_m + \alpha_e)^2}{16\pi^3 b^4 \ln(d/b) c^2} \left[\frac{N}{2} + \frac{N}{\alpha D} + \frac{e^{-\alpha DN} - 1}{(\alpha D)^2}\right]. \tag{35}$$

Fig. 3 compares, in a practical case, the "exact" coupling impedance (Eq. (18)) to its approximation (Eq. (35)); it grows as ω^2 except near frequencies satisfying the resonance condition (31), i.e. near are the peaks due to interference of backward propagating TEM waves in the coaxial. We see that Eq. (35) follows very well the exact one, at least far from resonances. In the low frequency range, we see the presence of a ripple with frequency given by (32); it is not considered in our approximation. Increasing N, the ripple becomes more and more negligible (with respect to other terms); moreover, using Eq. (35) leads to a remarkable simplification in the following computation allowing us to provide analytical results for the loss factor, as we will see in Sec. 3 where we show that the discrepancy presented in Fig. 3.b has no important effect.

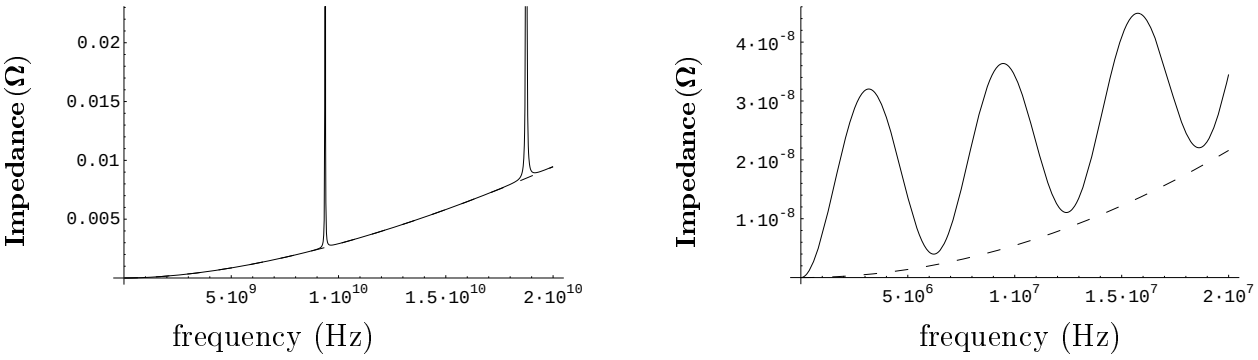

a) **b)**

Figure 3: Comparison between the exact expression for the coupling impedance (solid line) and the approximated one (dashed line), for 1500 rounded-end holes (that is a $\sim$ 24 m long device). In a) they can be hardly distinguished far from the peaks, while the difference is clear in the zoom at low frequencies b). All numerical values are taken from LHC parameters (see Table 1) and we have included the corrections due to the wall thickness (see Sec. 5)

2.3 Considering only the forward propagating TEM wave

Most of the literature includes only the forward propagating TEM wave in the coaxial region; the reason being that one can expect from it the major contribution to losses since it is travelling synchronous with the beam. Anyway this assumption is somehow arbitrary, since it is well known from the theory of directional microwave couplers (see for instance [19]) that the back-scattered wave plays its role and is usually exploited to synthetize the frequency behaviour of the directivity of the coupler. In this subsection we will compare this approach to our previous one, discussing the differences in our practical case (LHC).

Going back to the equivalent hole dipoles (Eq. (11)), neglecting the backward wave they become in this case:

$$M_\varphi(z_i) \simeq \alpha_m H_{0\varphi}(z_i) \left\{ 1 - j \frac{k_0}{4\pi b^2 \ln(d/b)} \left[\alpha_m + (\alpha_e + \alpha_m) F_i \, e^{-\alpha z_i} \right] \right\},$$
$$P_r(z_i) \simeq \varepsilon \alpha_e E_r(z_i) \left\{ 1 - j \frac{k_0}{4\pi b^2 \ln(d/b)} \left[\alpha_e + (\alpha_e + \alpha_m) F_i \, e^{-\alpha z_i} \right] \right\}. \qquad (36)$$

Thus, the coupling impedance is

$$Z(\omega) = j Z_0 \frac{\omega}{4\pi^2 b^2 c} N (\alpha_m + \alpha_e) +$$
$$+ Z_0 \frac{\omega^2}{16\pi^3 b^4 \ln(d/b) c^2} \left[N \left(\alpha_m^2 + \alpha_e^2 \right) + (\alpha_m + \alpha_e)^2 \sum_{h=1}^{N} F_h e^{-\alpha z_h} \right] \qquad (37)$$

and rewriting the real part for uniformly spaced holes, we get:

$$Z_{RE}(\omega) = Z_0 \frac{\omega^2}{16\pi^3 b^4 \ln(d/b) c^2} \left[N \left(\alpha_m^2 + \alpha_e^2 \right) + (\alpha_m + \alpha_e)^2 F(D, N, \alpha) \right], \qquad (38)$$

using the previous notations. The meaning of the two terms is clear: the non interacting holes (first one) and the interference effect due to forward propagating wave (second one).

Fig. 4 compares graphically this last equation with the exact one (Eq. (18)), in the LHC case. We remind that the resonant peaks (see Fig. 4.a) and the ripple (see Fig. 4.b) are due to the backward wave and so they are lost if we consider only the forward wave. The difference between the dashed and solid lines in of Fig. 4 and 3 is thus due to the constant term ($\propto N/2$) coming from $B(D, N, \alpha, \omega)$.

In conclusion we see that, at least for a LHC-like geometry, the main differences between considering and not considering the backward waves are at frequencies well above the cut-off of the bunch spectrum. Nevertheless also at low frequency (inside the bunch spectrum) there is a difference, even though not a substantial one.

It is worth noting that the relative influence of the back - forward waves depends on the hole shape, since the two terms are weighted with different functions of the polarizabilities. For instance, with circular holes the difference seen in Fig. 4.a (that is for rounded-end holes) is far less evident.

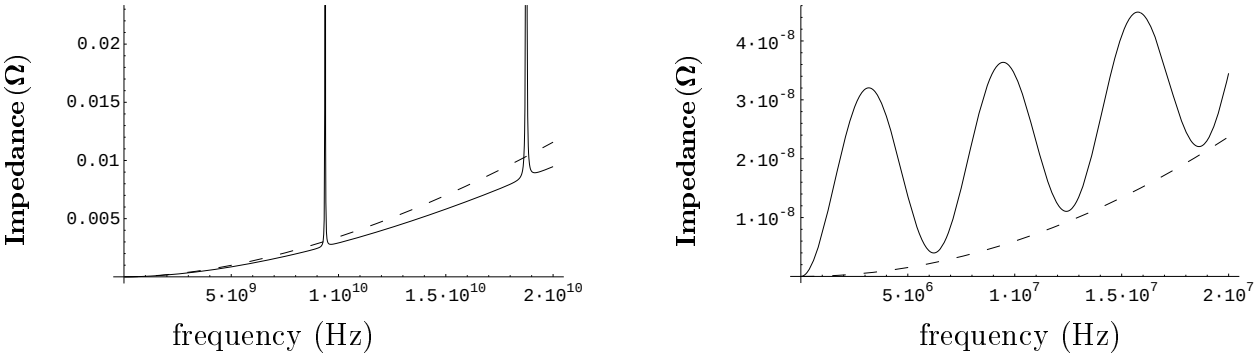

Figure 4: Comparison between the exact expression for the coupling impedance (solid line) and the one obtained considering only the forward propagating waves (dashed line), for 1500 rounded-end holes. b) is a detail at low frequencies. All numerical values are taken from LHC parameters (see Table 1) and we have included the corrections due to effects of the wall thickness (see Sec. 5)

3 Loss Factor

The loss factor is the energy lost by the bunch normalised to its charge squared; it depends on the coupling impedance and, for a Gaussian bunch of length σ, it can be written

$$k(\sigma) = \frac{1}{\pi} \int_0^\infty Z_{RE}(\omega)\, e^{-(\omega\,\sigma/c)^2} d\omega, \tag{39}$$

as we anticipated in Sec. 1.1.

First we present an approximation for bunch length bigger than the spacing among the holes and when the losses in the coaxial are negligible. Then we study the loss factor when there are ohmic losses giving analytical formulae and discussing the approximations involved.

3.1 Loss factor without attenuation

The integral in the loss factor can be performed analytically in this case, as reported in [2]. We now remind that formula and present some useful simplifications valid if the

length of the bunch is longer than the distance between the holes and for a large number of them.

The coupling impedance with no losses in the coaxial region is reported in Eq. (21); rewriting it with the help of Eq. (25) and performing the integration (39) yields

$$k(\sigma) = \frac{Z_0\sqrt{\pi}c}{128\pi^4 b^4 \ln(d/b)\sigma^3}\left[N^2(\alpha_m+\alpha_e)^2 + N(\alpha_m-\alpha_e)^2 - 2(\alpha_m-\alpha_e)^2 S\right], \qquad (40)$$

where

$$S = \sum_{h=1}^{N-1}(N-h)e^{-(hD/\sigma)^2}\left[2\left(\frac{D}{\sigma}h\right)^2 - 1\right]. \qquad (41)$$

As shown in Appendix B, for large N Eq. (41) can be approximated by

$$S \simeq \frac{1}{2}\left[N - \left(\frac{\sigma}{D}\right)^2\right] \qquad \text{if} \qquad \frac{D}{\sigma} < 1 \qquad (42)$$

since many terms of the sum are negligible; the loss factor (40) becomes

$$k(\sigma) \simeq \frac{Z_0\sqrt{\pi}c}{128\pi^4 b^4 \ln(d/b)\sigma^3}\left[N^2(\alpha_m+\alpha_e)^2 + \left(\frac{\sigma}{D}\right)^2(\alpha_m-\alpha_e)^2\right]. \qquad (43)$$

The dependence on N^2 takes into account interference effects between the holes and it is physically sound. Moreover, if

$$\frac{1}{N^2}\left(\frac{\sigma}{D}\right)^2\frac{(\alpha_m-\alpha_e)^2}{(\alpha_m+\alpha_e)^2} \ll 1,$$

the loss factor is proportional to N^2, although it is not N^2 times the loss factor of a single hole (that is proportional to $(\alpha_m^2+\alpha_e^2)$). In formulae

$$k(\sigma) \simeq \frac{Z_0\sqrt{\pi}c}{128\pi^4 b^4 \ln(d/b)\sigma^3}N^2(\alpha_m+\alpha_e)^2 \qquad \text{if} \qquad N \gg A\frac{\sigma}{D} \qquad A = \frac{(\alpha_m-\alpha_e)}{(\alpha_m+\alpha_e)}. \quad (44)$$

In the case of circular holes in a thin wall, for example, $A = 3$.

The result of Eq. (44) shows the importance of the interference effects between the holes due to the presence of the TEM field in the coaxial region. These effects are not always considered in the literature and they cause the total loss factor to depend on N^2; for example [9] proposes, for the same geometry, to estimate the total energy lost by the bunch by taking N times the loss factor for a single hole.

3.2 Attenuation due to ohmic losses

We have studied the impedance for an attenuation source in the coaxial region such that the field propagating there remains essentially TEM shaped; this is for instance the case of distributed dielectric losses.

In first approximation, also the effect of lossy walls can be treated in this way by using the following attenuation constant [4]

$$\alpha(\omega) = a\sqrt{\omega} \qquad \text{with} \qquad a = \frac{1}{2\,Z_0\,\ln(d/b)}\left(\frac{\rho_b}{b} + \frac{\rho_d}{d}\right)\sqrt{\frac{\mu}{2}} \qquad (45)$$

where ρ_b (ρ_d) is the resistivity of the cylindrical surface of radius b (d). Although it is only an approximation, this approach is widely used in the estimation of losses in high power RF transmission lines [15].

Using Eq. (45) in Eq. (18) yields the real part of the coupling impedance for this particular source of losses and then performing the integral of Eq. (39), we get the loss factor. Unfortunately this can not be done analytically and we use now the approximations for the coupling impedance discussed earlier, namely the one including only the forward propagating TEM wave of Eq. (38) and the one including everything but the peaks of the impedance, see Eq. (35).

First of all, to check their validity, we focus on the function under the integral, that is Z_{RE} times the bunch current in absolute squared value (i.e. the Gaussian of Eq. (39) modulo some constant), that is the spectrum in frequency of the power lost by the bunch.

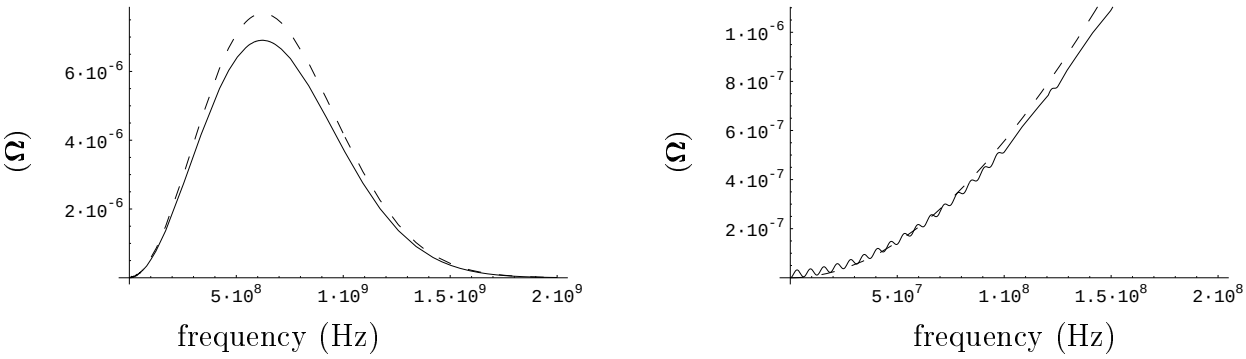

a) **b)**

Figure 5: Function under the integral of the loss factor using the exact expression for the coupling impedance (solid line) and considering only the forward propagating waves (dashed line), for 1500 rounded-end holes. b) is a detail at low frequencies. All numerical values are taken from LHC parameters (see Table 1) and we are including the corrections due to effects of the wall thickness (see Sec. 5)

Fig. 5 shows the function under the integral, when we include only the effect of forward propagating waves, namely using Eq (38) for the coupling impedance; Fig. 5.b shows the detail at low frequency, where the ripple is again due to interference effects associated to backward scattered waves. Thus there is a difference between the exact and the approximated one, but it is not dramatic and it leads to an overestimated value of the loss factor.

On the other hand, Fig. 6 compares the exact value of the spectrum of the power lost by the beam with the one we got by using Eq. (35). The difference can not be seen in a wide frequency range (Fig. 6.a), but is clear at low frequencies even if it is very small.

The previous curves correspond to a fixed number of holes ($N = 1500$ that is a section 24 m long); decreasing the number of holes increases the magnitude of the ripple (as seen in Sec. 2.2.2) and our approximate formulae lose in accuracy, even though the result remains acceptable, as we will show.

Thus, both approximations are not far from reality, although they do not take into account the sharp peaks of the impedance; infact those peaks are outside the relevant spectrum of the bunch.

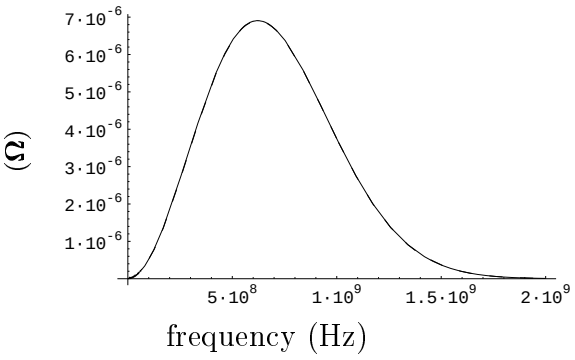

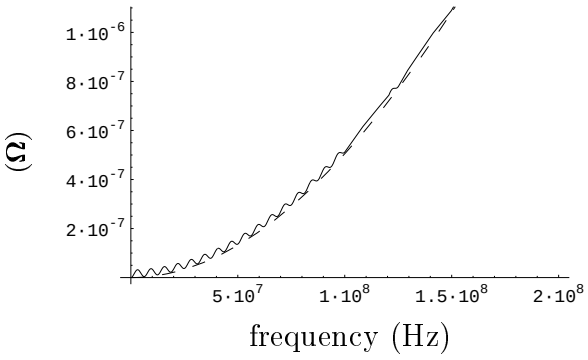

a) **b)**

Figure 6: Function under the integral of the loss factor using the exact expression for the coupling impedance (solid line) and the approximation valid far from the frequencies of its peaks (dashed line), for 1500 rounded-end holes. In a) they can be hardly distinguished, while the difference is clear in the detail at low frequencies b). All numerical values are taken from LHC parameters (see Table 1) and we are including the corrections due to effects of the wall thickness (see Sec. 5)

We now use the two approximate formulae for the coupling impedance, Eqs. (35) and (38), to derive analytically the loss factor and we compare it with numerical results using the exact impedance.

Since

$$I_1 = \int_0^\infty \omega^2 e^{-(\omega\sigma/c)^2} d\omega = \frac{\sqrt{\pi}}{4}\left(\frac{c}{\sigma}\right)^3, \quad I_2 = \int_0^\infty \omega^{3/2} e^{-(\omega\sigma/c)^2} d\omega = \frac{1}{2}, \left(\frac{5}{4}\right)\left(\frac{c}{\sigma}\right)^{5/2},$$

$$I_3 = \int_0^\infty \omega \left(e^{-aDN\sqrt{\omega}} - 1\right) e^{-(\omega\sigma/c)^2} d\omega =$$
$$-\frac{c^2}{2\sigma^2} + \frac{c^2}{2\sigma^2}\,{}_1F_3\left(1; \frac{1}{4}, \frac{1}{2}, \frac{3}{4}; \frac{a^4c^2}{256\sigma^2}N^4D^4\right) - , \left(\frac{5}{4}\right)\frac{a}{2}\left(\frac{c}{\sigma}\right)^{5/2}\,{}_0F_2\left(; \frac{1}{2}, \frac{3}{4}; \frac{a^4c^2}{256\sigma^2}N^4D^4\right) ND +$$
$$+\frac{\sqrt{\pi}a^2c^3}{8\sigma^3}\,{}_0F_2\left(; \frac{3}{4}, \frac{5}{4}; \frac{a^4c^2}{256\sigma^2}N^4D^4\right) N^2D^2 - , \left(\frac{3}{4}\right)\frac{a^3}{16}\left(\frac{c}{\sigma}\right)^{7/2}\,{}_0F_2\left(; \frac{5}{4}, \frac{3}{2}; \frac{a^4c^2}{256\sigma^2}N^4D^4\right) N^3D^3,$$

where ${}_pF_q$ is the generalised hypergeometric series [11], we get

$$k(\sigma) = \frac{Z_0\left(\alpha_m + \alpha_e\right)^2}{16\pi^4 b^4 \ln\left(d/b\right)c^2}\left[\frac{\sqrt{\pi}}{8}\left(\frac{c}{\sigma}\right)^3 N + \frac{1}{2}, \left(\frac{5}{4}\right)\frac{c^{5/2}}{aD\sigma^{5/2}}N + \frac{I_3}{a^2D^2}\right]. \tag{46}$$

In the limit of large N the third term in the square brackets becomes negligible with respect to the other two, as it is clear from the definition of I_3.

The behaviour of the loss factor as a function of the length of perforated screen L_d is shown in Fig. 7. When L_d (or N) is small, the holes interfere as if no attenuation was present in the coaxial region and the loss factor grows quadratically (Fig. 7.a). As the length increases, not all the holes interact with each other since the attenuation damps the field; if two holes are too far away their contribution to the losses is simply the sum of the contributions of the two non interacting holes. Thus, for large lengths the loss

factor grows linearly, as seen in Fig. 7.b. The dashed line is the loss factor accounting only for forward propagating waves in the coaxial, while the solid one includes also the back-scattered waves; the dots are numerical values of the loss factor integral including the exact impedance of Eq. (18). The agreement of the results is good: at the length of 15 m the error between the solid line and the numerical result is of 0.3% while for the dashed it is 17%. Going to small lengths, our approximations loses in accuracy since the

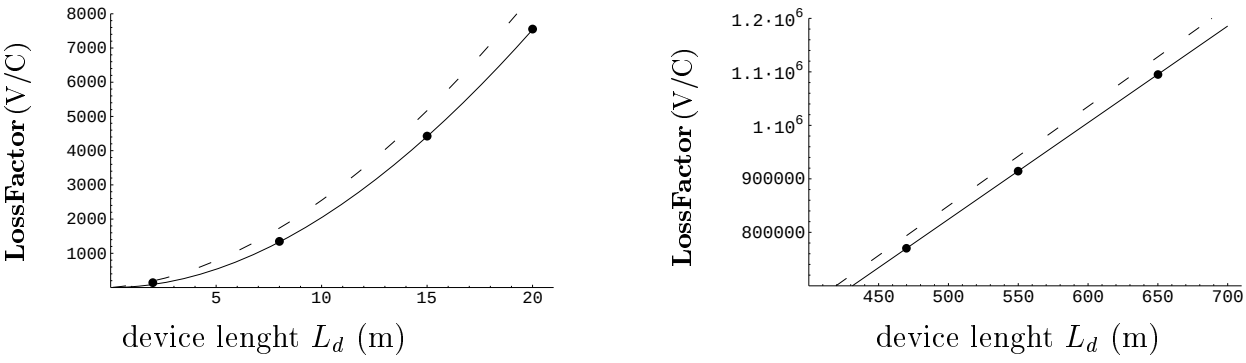

a) **b)**

Figure 7: Loss factor as a function of the length of the beam screen. The dots are obtained numerically using the exact coupling impedance, while the lines are the analytical approximations including only forward waves (dashed) and the impedance without the peaks. All numerical values are taken from LHC parameters (see Table 1) and we are including the corrections due to effects of the wall thickness (see Sec. 5)

term B of Eq. (18) can not be approximated simply by a constant, as already said. Thus we expect a bigger error for small length, as we see in Fig. 8.

4 Power lost per unit length

The excited TEM field dissipates power on the walls of the coaxial region, causing heating of the cold bore; thus, providing an estimate of such power is essential in the project of the LHC.

We first discuss the connection between the power per unit length and the loss factor, then we provide an analytical formula, using previous results for $k(\sigma)$. To better understand and to achieve handy formulae, we focus on the two limiting behaviours (namely for very small and infinite lengths) and define a boundary between these two. Eventually we treat the case of more than one hole per cross section.

The energy lost by the bunch in a section of length $L_d = ND$ is the loss factor times Q^2, where Q is the charge of the bunch. If the inner part of the beam screen is a perfect conductor, all the energy lost by the bunch is transferred to the propagating field (energy conservation law). Dividing that energy by the time the bunch takes to cover the length L_d (i.e. L_d/c for relativistic bunches) yields the power flowing in the coaxial. The ratio between this and again the length L_d is defined as the power per unit length and takes into account the effect of a single bunch travelling in the inner pipe. If we assume that the total power is the sum of the power due to each of the n_b bunches in a length L_d, we get the expression of the power per unit length given in Sec. 1.1:

$$P = n_b \frac{c\, Q^2\, k\,(\sigma)}{L^2} = \frac{c\, Q^2\, k\,(\sigma)}{S_b\, L}, \tag{47}$$

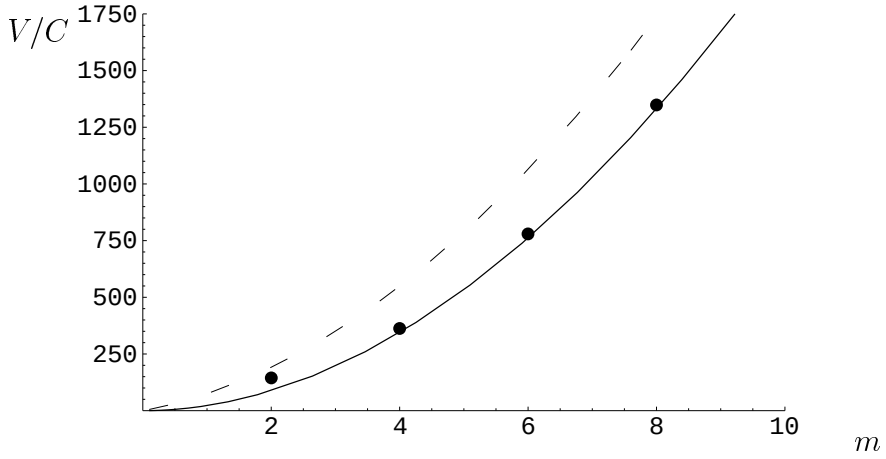

Figure 8: Loss factor as a function of the length of the beam screen. The dots are obtained numerically using the exact coupling impedance, while the lines are the analytical approximations including only forward waves (dashed) and the impedance without the peaks (solid). All numerical values are taken from LHC parameters (see Table 1) and we are including the corrections due to effects of the wall thickness (see Sec. 5)

where S_b is the bunch spacing ($S_b = L_d/n_b$).

In Sec. 3.1 we derived and discussed an analytical expression for $k(\sigma)$ that was found to be a very good approximation of the real one; inserting it in Eq. (47) yields

$$P = \frac{(\alpha_m + \alpha_e)^2}{16\,\pi^4\,b^4\,\ln(d/b)\,S_b\,D}\left[\frac{\sqrt{\pi}}{8}\frac{Z_0\,Q^2\,c^2}{\sigma^3} + \frac{1}{2},\left(\frac{5}{4}\right)\frac{Z_0\,Q^2\,c^{3/2}}{a\,D\,\sigma^{5/2}} + \frac{1}{N}\frac{Z_0\,Q^2\,I_3}{a^2\,D^2\,c}\right]. \qquad (48)$$

A typical behaviour of P with the device length L ($L = ND$) is drawn in Fig. 9, for the nominal LHC case. The distance between the holes D and their number N are such that the surface covered by the holes is the 4.4% of the total surface of the pipe.

As shown in Fig. 9, there are two simple limiting behaviours of P: it saturates for very long devices, while it grows linearly when the length L_d is small.

In the limit of large L_d, Eq. (48) becomes constant:

$$P_\infty = \lim_{N\to\infty} P = \frac{(\alpha_m + \alpha_e)^2}{16\,\pi^4\,b^4\,\ln(d/b)\,S_b\,D}\left[\frac{\sqrt{\pi}}{8}\frac{Z_0\,Q^2\,c^2}{\sigma^3} + \frac{1}{2},\left(\frac{5}{4}\right)\frac{Z_0\,Q^2\,c^{3/2}}{a\,D\,\sigma^{5/2}}\right]. \qquad (49)$$

The physical reason is that over a certain length, the number of holes interacting with each other is fixed by the attenuation of the field: increasing the number of holes (i.e. L_d) doesn't change the losses per unit length. In this range the loss factor goes linearly with L_d, see Fig. 7.b.

On the contrary, the attenuation doesn't dump the field efficiently in short lengths; the loss factor for such lengths grows parabolically, see Fig. 7.a. We can study this limit as if there were no attenuation and using Eq. (44) for the loss factor yields

$$P_{lin} = \frac{\sqrt{\pi}}{128\,\pi^4}\,\frac{Z_0\,Q^2\,c^2}{\sigma^3}\,\frac{(\alpha_m + \alpha_e)^2}{b^4\,D\,S_b\,\ln(d/b)}\,N. \qquad (50)$$

It grows linearly with N (or L_d) because of the interference effect among all the holes: each hole interacts with all the others. This is actually an approximation of Eq. (48) for short L_d, but it gives a simple formula physically sound.

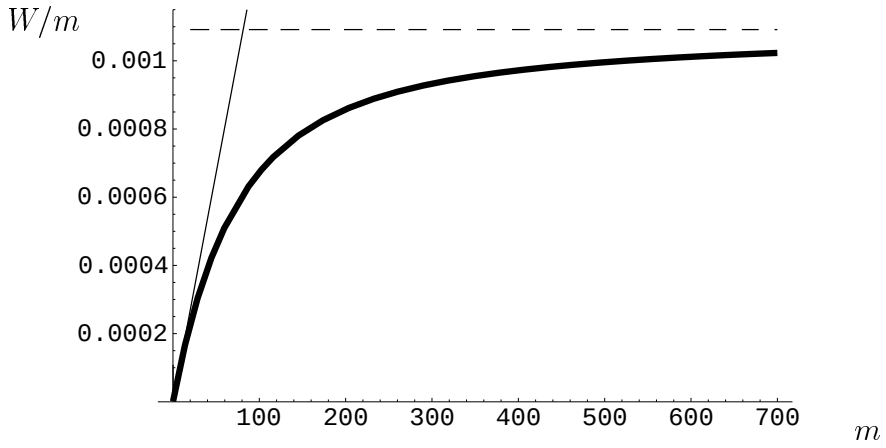

Figure 9: Power per unit length (W/m) as a function of the length of the beam screen (m). The thick line is the exact value, while the solid thin line accounts for the case without losses; the dashed one is the limit value, reached at very long length. All numerical values are taken from LHC parameters (see Table 1) and we are including the corrections due to effects of the wall thickness (see Sec. 5); the number and the distance between the rounded-end slots are chosen such that the surface covered by the holes is 4.4% of the surface of the pipe.

It is useful to define a boundary between this two behaviours, namely the linear and the saturated one: below that we can consider the power per unit length to grow linearly with L_d, while above we can assume it constant and equal to its saturation value P_∞. Therefore, we define L_α as the length such that the linear approximation P_{lin} crosses the limit value P_∞, that is

$$L_\alpha = D + \frac{4}{\sqrt{\pi}}\,,\left(\frac{5}{4}\right)\frac{\sqrt{\sigma}}{a\sqrt{c}} = D + \frac{4}{\sqrt{\pi}}\,,\left(\frac{5}{4}\right)\frac{1}{\alpha\left(\omega_c\right)}, \tag{51}$$

where $\omega_c = 2\pi f_c$ and f_c is the cut-off frequency of the Gaussian spectrum of the bunch. Approximately we can say that after L_α, the power per unit length reaches its saturation value.

L_α depends on the the attenuation α, on the bunch length and on the spacing among the holes. The dependence on D is not relevant for our practical case (LHC) because the second term is orders of magnitude bigger; that dependence simply states that for very strong attenuation (i.e. $\alpha \to \infty$) the saturation value is reached at lengths equal to the spacing among the holes. This is not surprising, because (see Sec. 2.1.2) in this case the holes do not interact; consequently the coupling impedance (and thus the loss factor) is linear in L_d (or in N) and the power lost per unit length is constant. The other term is proportional to the inverse of the attenuation constant computed at the cut-off frequency f_c; it is not exactly $1/\alpha\left(\omega_c\right)$ (as we could expect) since the loss factor (and P) is an average on all the frequencies. For the nominal values of the LHC (see Table 1) L_α is about 80 m.

Up to now we have assumed a single line of holes drilled with constant spacing equal to D. If there are more than one hole for a given longitudinal position, we have to multiply our formulae by the number of holes per cross section N_b squared. Infact holes in the same section always interfere constructively, since both the charge field and the TEM one are

constant in the azimuthal coordinate and thus they are excited with the same phase. Anyway in the example shown in Fig. 9, where the constraint is the pumping surface, increasing the number of pumping holes per cross section N_b implies an increase of the distance between the holes D. Now, the dominant term of Eq. (49) for P_∞, is proportional to N_b/D squared and thus its value doesn't change if we increase the number of holes per cross section. The same reasoning holds for Eq. (50), since if we rewrite it in terms of the length L_d ($N = L/D$), P_{lin} depends again on N_b/D squared.

5 The effect of wall thickness

Up to now, we have neglected the effect of the finite thickness of the wall: it changes the problem geometry and introduces an attenuation for the fields in the holes.

About the change of the problem geometry, we should notice that, because of the thickness of the wall, the radius of the pipe "seen" by the beam is different from the radius of the inner tube of the coaxial structure. Calling b_1 and b_2, respectively the inner and the outer radius of the beam pipe (see Fig. 1), one can show that the factor b^4 in the denominator of the expressions of impedance and loss factor has to be replaced by the product $b_1^2 b_2^2$. A similar argument holds for the $\ln(d/b)$ that becomes $\ln(d/b_2)$.

The most important correction is on the polarizabilities since the fields are exponentially attenuated going through the holes. We can imagine that the outer magnetic (electric) polarizability scales as the magnetic (electric) field going into a cylindrical waveguide of the same cross-section of the hole. Because the hole is supposed to be very small with respect to λ (since we are dealing with static polarizabilities), all the modes of these equivalent wave-guides are below cut-off and their attenuation is exponential with the thickness. If the latter is sufficiently large with respect to a typical dimension of the hole, only the contribution of the less attenuated mode (i.e. the fundamental one of the wave guide corresponding to the hole) will affect the scaling of thin wall polarizabilities. Although only approximate, this approach, presented and discussed in [16], has been adopted in [2] and also in [9].

For circular holes of radius R these modified polarizabilities are [2]

$$\begin{aligned} \tilde{\alpha}_m &= C_M\, \alpha_m\, e^{-2.405\, T/R} \qquad \text{with} \quad C_M = 0.84 \quad \text{and} \quad \alpha_m = \frac{4}{3} R^3, \\ \tilde{\alpha}_e &= C_E\, \alpha_e\, e^{-1.841\, T/R} \quad \text{with} \quad C_E = 0.83 \quad \text{and} \quad \alpha_e = -\frac{2}{3} R^3, \end{aligned} \tag{52}$$

where $T = b_2 - b_1$ is the wall thickness and the numerical values for C_E and C_M are taken from [16]. The exponential factor is clearly related to the attenuation of fields due to the thickness. Performing the overlapping integral between the source field and the modes of the cylindrical wave-guide equivalent to the hole yields the appropriate values for C_E and C_M; due to the normalisation of wave guide modes they must be always less than 1.

The pumping holes foreseen for the beam screen of LHC are rounded-end shaped. Their "thin wall" polarizabilities are [14]

$$\begin{aligned} \alpha_m &= \frac{\pi}{16} W^2 L \left[1 + 0.3577 \frac{W}{L} - 0.0356 \left(\frac{W}{L} \right)^2 \right], \\ \alpha_e &= -\frac{\pi}{16} W^2 L \left[1 - 0.5663 \frac{W}{L} + 0.1398 \left(\frac{W}{L} \right)^2 \right], \end{aligned} \tag{53}$$

where W is the width and L is the length of the holes. In case of finite thickness of the

wall they can be corrected as in [3], that is

$$\tilde{\alpha}_m = C_M\,\alpha_m\,e^{-\upsilon T} \quad \text{with} \quad \upsilon = -\frac{\pi}{W},$$
$$\tilde{\alpha}_e = C_E\,\alpha_e\,e^{-\gamma T} \quad \text{with} \quad \gamma = -\pi\sqrt{\frac{1}{L^2}+\frac{1}{W^2}}; \tag{54}$$

where the value proposed (using numerical results) for $C_M = C_E$ is 0.61. We should notice that γ and υ are the attenuation constants of rectangular wave-guide modes, not of "rounded-end" ones (that can not be expressed analytically). The error introduced using the "rectangular" constants is negligible. Moreover, the ratio between the thickness of the wall and the dimensions of the holes in LHC allows us to use Eqs. (54) that clearly take into account only the effects of one TE and one TM mode of a rectangular waveguide.

In a following section (Sec. 7), where are presented numerical estimates for LHC with rounded-end slots, we will take the maximum possible value for C_M and C_E, that is 1, as stated before.

6 Discussion

We now compare our results to a previous paper [4] which reports on some measurements done on a 2 m long model of the LHC vacuum chamber and tries to interpret them with the help of a simplified model. In Sec. 6.1 we consider the case of negligible attenuation (i.e. small L_d), while in Sec. 6.2 we discuss P_∞.

In [4] they study essentially the build up of the forward TEM wave, that is the main source of losses since it is synchronous with the beam. They derived a simple equation for the amplitude of the field in the coaxial with the holes described again by means of polarizabilities. Only circular holes were treated and the expression of the polarizabilities are essentially the same ones given in Eq. (52), including the dependence on the wall thickness. They focus on the transmission coefficient (i.e. the ratio between the maximum absolute value of the field in the coaxial and the field in the beam pipe) in the two limiting cases: ignoring the attenuation (suitable for length much smaller than L_α) and for infinite length. The first case is also compared to measurements showing the theoretical values are about a factor two below the measured ones. The effects of non interacting holes and of the backward propagating waves were ignored. These two contributes are anyway marginal, at least for the LHC: the first one is important only when the attenuation is very high ($\alpha \to \infty$), while the backward waves give remarkable contributions only at very high frequencies, at least for the LHC.

6.1 Forward transmission coefficient

The forward transmission coefficient is given by

$$G(\omega) = \left|\frac{E_{sr}}{E_0}\right| \tag{55}$$

where $E_{sr}(z)$ is the electric field radiated by all the holes in the coaxial region and the source field E_0 is that one of a relativistic charge given in Eq. (2).

$E_{sr}(z)$ is the superposition of the field radiated by each hole. To measure the overall transmission coefficient we will consider the field at the end of the rows of holes and Eq. (5) becomes

$$E_{sr}\,(z) = \sum_{h=1}^{N} E_r\,(z, z_h) = e^{-jk_0 z} \sum_{h=1}^{N} c_{0i} e_{0r} e^{jk_0 z_i}, \tag{56}$$

since $z > z_h \quad \forall\, h \quad (h = 1, \ldots, N)$; the coefficients c_{0i} are given by Eq. (7). We recall that we are considering fields in the frequency domain. Inserting Eqs. (6) and (7) into Eq. (56) yields

$$E_{sr}(z) = j\frac{Z_0\ \omega}{4\pi b^2 \ln(d/b)} e^{-jk_0 z} \sum_{i=1}^{N} \left[\frac{M_\varphi(z_i)}{c} + P_r(z_i)\right] e^{jk_0 z_i} \tag{57}$$

and eventually we get, from Eq. (4),

$$E_{sr}(z) = \frac{q\, Z(\omega)}{2\, b\, \ln(d/b)} e^{-j\frac{\omega}{c}z}. \tag{58}$$

The forward transmission coefficient is then

$$G(\omega) = \frac{\pi}{\ln(d/b)} \frac{|Z(\omega)|}{Z_0}. \tag{59}$$

Since the absolute value of the coupling impedance is dominated by its imaginary part (given in Eq. (14)), the coefficient $G(\omega)$ becomes

$$G(\omega) \simeq N \frac{\omega}{4\,\pi\, b_1\, b_2 \ln(d/b_2)\, c} \left|\tilde{\alpha}_m + \tilde{\alpha}_e\right|, \tag{60}$$

where we have already included the effect of the wall thickness using b_1, b_2 and the polarizabilities for "thick" wall $\tilde{\alpha}_m$ and $\tilde{\alpha}_e$, as previously discussed (Sec. 5). This result is identical to the analytical expression derived in [4], since when there is no attenuation, the effect of the forward propagating wave (the only considered in [4]) dominates.

6.2 Power lost per unit length: the asymptotic value

The saturation value of the power lost per unit length derived in [4] and expressed in our notation is

$$\widehat{P}_\infty = \frac{1}{2},\ \left(\frac{5}{4}\right) N_b^2 \frac{Z_0\, Q^2\, c^{3/2}\ \left(\tilde{\alpha}_m + \tilde{\alpha}_e\right)^2}{16\,\pi^4\, b_1^2\, b_2^2 \ln(d/b_2)\, S_b\, a\, D^2\, \sigma^{5/2}}; \tag{61}$$

It is actually the second term of Eq. (49) that is the one accounting for the effect of the forward propagating TEM field, having included the changes discussed in Sec. 5 because of the thick wall and considering N_b holes per cross section.

It is worth noting that in the complete expression the term accounting for the effect of non interacting holes and the one due to the backward wave have different signs and almost cancel each other giving the first term in the square brackets of Eq. (49). This explains why Eq. (61) gives almost exactly the value of the plateau in Fig. 9.

7 LHC case

All the numerical examples given before are done with LHC nominal parameters, in particular assuming rounded-end slots and the attenuation due to ohmic losses in the walls of the coaxial region (see Table 1 for numerical values).

The maximum power loss per unit length in the nominal case is 1.1 mW/m and L_α is 81.5 m, as we see in Fig. 9. Probably the pure coaxial structure will be limited only to sections shorter than L_α since all the devices such as pumps, kickers, ... will be installed outside the beam screen, resulting in different geometries for the "coaxial" region. Therefore the linear approximation P_{lin} could be the most useful in practical cases.

In the original proposal circular holes were foreseen; P has the same behaviour (L_α doesn't change), but its value is scaled by

$$\frac{(\tilde{\alpha_m} + \tilde{\alpha_e})^2_{circ}}{(\tilde{\alpha_m} + \tilde{\alpha_e})^2_{round}} \frac{N^2_{circ}}{N^2_{round}} \simeq 13, \tag{62}$$

if we assume the radius of the holes $R = W/2$, the nominal values for L, W, and T and if we put $C_M = C_E = 1$ for rounded-end holes. N_{round} (N_{circ}) are the number of rounded-end (circular) holes covering 4.4% of the beam screen surface. The value estimated in this way agrees with the previous estimate [13].

In Table 2 we report some values for two different (and relevant) device lengths: the first is the dipole length (14 m) while the second is $L_d \gg L_\alpha$ (i.e. the limiting value P_∞). The critical parameters, on which the final result depends, are the thickness of the screen and the width of the slots W as well as their shapes: small changes on them imply large changes on the final value of P.

It is worth noting that the specific power given by Eq. (47) is dissipated in the coaxial because of the ohmic losses in the walls. It will be dissipated partly on the inner wall and partly on the outer one. The cold bore heating depends only on the power dissipated in the outer wall; assuming the same conductivity for both walls, we should then scale the previous result by the geometric factor $b_2/(b_2 + d) \simeq 45\%$, as stated in [4].

	Rounded-end slots		Circular holes	
	@ Dipole	P_∞	@ Dipole	P_∞
$W = 1.5\,\mathrm{mm}$, $L = 8.0\,\mathrm{mm}$, $T = 1.0\,\mathrm{mm}$	0.19	1.1	2.49	14.5
$\boldsymbol{W} = 2.0\,\mathrm{mm}$, $L = 8.0\,\mathrm{mm}$, $T = 1.0\,\mathrm{mm}$	1.65	9.5	13.2	76.9
$\boldsymbol{W} = 3.0\,\mathrm{mm}$, $L = 8.0\,\mathrm{mm}$, $T = 1.0\,\mathrm{mm}$	22.3	129.6	85.6	497.1
$W = 1.5\,\mathrm{mm}$, $L = 8.0\,\mathrm{mm}$, $\boldsymbol{T} = 0.5\,\mathrm{mm}$	1.22	7.0	21.4	124.3

Table 2: Power lost per unit length (mW/m) in the LHC case for different length and different hole shapes. The **bolded** letters stress the changed value in each row with respect to the first row (nominal values).

8 Conclusions

Analytical formulae are given for coupling impedance, loss factor and power lost per unit length for many holes in a coaxial liner and in presence of attenuation in the coaxial region. These results confirm and generalise previous ones; they are also helpful to understand the most relevant physical parameters in the design of the LHC beam screen.

Interference effects between the holes (not always considered in the literature) are mainly responsible for the beam energy loss. The attenuation in the coaxial region (at least the ohmic one in LHC) reduces them, but only over long distances (we find $\simeq 80$ m for the LHC).

The coupling impedance for equally spaced holes is parabolic in frequency with superimposed interference peaks that are sharp and high. Those are nevertheless out of the bunch spectrum in the LHC and are also reduced by the foreseen randomisation: they don't seem to be dangerous for beam stability.

The power per unit length dissipated in the cold bore (≤ 1.1 mW/m for nominal parameters) is not affected by the randomisation of the position of the holes. It depends

strongly on the shape and dimensions of the holes. In particular the critical parameters are the width of the hole W and the wall thickness T: increasing the first or decreasing the second has to be done carefully to avoid too much power flowing in the coaxial region and heating the cold bore. The fraction of this power dissipated in the beam screen is less important since it has to be added to other sources of heating, for instance the incoherent synchrotron radiation (estimated [13] around 206 mW/m), that impose more serious limits. Moreover many devices will be installed outside the beam pipe; they will interrupt the ideal coaxial geometry to lengths shorter than L_α where the losses are linear with the device length and are remarkably smaller (0.19 mW/m for a dipole length).

9 Acknowledgements

I would like to thank F. Ruggiero who contributed substantially to this paper, giving very helpful comments and suggestions. Many thanks to L. Palumbo and S. De Santis for their continuous, fruitful collaboration. I am also grateful to the AP group of the SL Division at CERN for its hospitality during the course of my work.

References

[1] S. De Santis, M. Migliorati, L. Palumbo and M. Zobov, *Coupling impedance of a hole in a coaxial beam pipe*, Phys. Rev. **E**, **54**, 1996, pp. 800–805.

[2] S. De Santis, A. Mostacci and L. Palumbo, *Interference effects on the coupling impedance of many holes in a coaxial beam pipe*, Phys. Rev. **E**, **56**, 1997, pp. 5990–5995.

[3] S. De Santis, A. Mostacci, L. Palumbo and B. Spataro, *Analytical expressions for the coupling impedance of a long narrow slot in a coaxial beam pipe*, to be published in Phys. Rev. **E** (1998).

[4] F. Caspers, E. Jensen and F. Ruggiero, *Impedance measurements for the pumping holes in the LHC liner*, CERN SL/92-15 (DI), PS/92-24 (RF/AR), LHC note 186 (1992) and Proc. EPAC Conference, Berlin, 1992, eds. H. Henke, H. Homeyer and Ch. Petit-Jean-Genaz (Editions Frontières, Singapore, 1992), pp. 889–891.

[5] H.A. Bethe, *Theory of diffraction by small holes* , Phys. Rev., **66**, 1944, pp. 163–182.

[6] S.S. Kurennoy, *Coupling impedance of pumping holes*, Particle Accelerators, **39**, 1992, pp. 1–13.

[7] G.V. Stupakov, *Coupling impedance of a long slot and an array of slots in a circular vacuum chamber*, Phys. Rev. **E**, **51**, 1995, pp. 3515–3521.

[8] A.V. Fedotov and R.L. Gluckstern, *Analytic and numerical analysis of the longitudinal coupling impedance of a rectangular slot in a thin coaxial liner*, Phys. Rev. **E**, **56**, 1997, pp. 3583–3601.

[9] A.V. Fedotov and R.L. Gluckstern, *Impedance and resonance issues for a long rectangular slot in a coaxial liner*, Phys. Rev. **E**, **56**, 1997, pp. 7217–7222.

[10] L. Palumbo, V.G. Vaccaro and M. Zobov, *Wake fields and impedance*, CAS Cern Accelerator School, Advanced school on accelerator physic, Rhodes 1994, LNF-94/041 (1994).

[11] I.S. Gradshtein and I.M. Ryzhic, *Table of integrals, series and products. Corrected and enlarged edition*, (Accademic Press, New York, 1980), p. 1045.

[12] R.E. Collin, *Field theory of guide waves*, 2nd ed., (IEEE, New York, 1991).

[13] F. Ruggiero, *Single-beam collective effects in the LHC*, CERN SL/95-09 (AP), LHC note 313 (1995) and Proc. Workshop on Collective Effects in Large Hadron Collid-

ers, Montreux, 1994, eds. E. Keil and F. Ruggiero (Particle Accelerators, **50**, 1995), pp. 83–104.
[14] S.S. Kurennoy, *Impedance iussues for the LHC beam screen*, Proc. Workshop on Collective Effects in Large Hadron Colliders, Montreux, 1994, eds. E. Keil and F. Ruggiero (Particle Accelerators, **50**, 1995), pp. 167–104.
[15] R.K. Cooper, *High power RF trasmission*, CAS Cern Accelerator School, RF Engineering for Particle Accelerators, Oxford 1991, CERN 92-03 (1992), pp. 264–265.
[16] N.A. McDonald, *Electric and magnetic coupling through small apertures in shield walls of any thickness*, IEEE Trans. Microwave Theory Tech., **MTT-20**, no. 10, 1972, pp. 689–695.
[17] The LHC Study Group, *The Large Hadron Collider, conceptual design*, CERN/AC/95-05 (LHC), 20 October 1995.
[18] L. Palumbo, *Private communication* (March 1998).
[19] R.S. Elliot, *An introduction to guided waves and microwave circuits*, (Prentice-Hall, Inc., New Jersey, 1993).

Appendix A

We now outline briefly the most important steps leading from Eq. (9) to Eq. (11); we take as an example the magnetic dipole moment M_φ, but also for P_r the procedure is essentially the same.

Substituting Eq. (10) in the RHS of Eqs. (9), we get the first order solution $M_\varphi^{(1)}$, discussed in Sec. 2.1.1:

$$M_\varphi^{(1)}(z_h) = \alpha_m \left[H_{0\varphi} e^{-jk_0 z_h} - j\frac{\omega}{2}\mu h_{0\varphi}^2 \sum_{k=1}^{N} \alpha_m H_{0\varphi} e^{-jk_0 z_k} e^{-jk_c|z_h - z_k|} + \right.$$
$$\left. + j\frac{\omega}{2} h_{0\varphi} e_{0r} \sum_{k=1}^{N} sgn(k-h)\varepsilon\alpha_e E_{0r} e^{-jk_0 z_k} e^{-jk_c|z_h - z_k|} \right]. \qquad (63)$$

Since

$$E_{0r} = Z_0 H_{0\varphi} = Z_0 \frac{q}{2\pi b} \qquad \mu h_{0\varphi}^2 H_{0\varphi} = \frac{\mu}{Z_0} \frac{H_{0\varphi}}{2\pi b^2 \ln(d/b)}$$
$$\varepsilon h_{0\varphi} e_{0r} E_{0r} = \varepsilon Z_0 \frac{H_{0\varphi}}{2\pi b^2 \ln(d/b)}, \qquad \frac{\mu}{Z_0} = \varepsilon Z_0 = \frac{1}{c}$$

it yields

$$M_\varphi^{(1)}(z_h) = \alpha_m H_{0\varphi} \left[e^{-jk_0 z_h} - j\frac{k_0}{4\pi b^2 \ln(d/b)} \alpha_m \sum_{k=1}^{N} e^{-jk_0 z_k - jk_c|z_h - z_k|} + \right.$$
$$\left. + j\frac{k_0}{4\pi b^2 \ln(d/b)} \alpha_e \sum_{k=1}^{N} sgn(k-h) e^{-jk_0 z_k - jk_c|z_h - z_k|} \right]. \qquad (64)$$

After some algebraic manipulation, recalling that $k_c = k_0 - j\alpha$ and that $sgn(k-h) = 0$ if $k = h$ we find

$$M_\varphi^{(1)}(z_h) = \alpha_m H_{0\varphi} \left[e^{-jk_0 z_h} - \alpha_m T_1 - \alpha_m T_2 - \alpha_e T_3 + \alpha_e T_4 \right] \qquad (65)$$

where

$$T_1 = j\frac{k_0}{4\pi b^2 \ln(d/b)} e^{-jk_0 z_h} \sum_{k=1}^{h} e^{\alpha(z_k - z_h)},$$

$$T_2 = T_4 = j\frac{k_0}{4\pi b^2 \ln(d/b)} \sum_{k=h+1}^{N} e^{-j2k_0 z_k} e^{-\alpha(z_k - z_h)} e^{jk_0 z_h} = j\frac{k_0}{4\pi b^2 \ln(d/b)} e^{-jk_0 z_h} \sum_{w=1}^{N-h} e^{-(j2k_0+\alpha)(z_{w+h}-z_h)},$$

$$T_3 = j\frac{k_0}{4\pi b^2 \ln(d/b)} e^{-jk_0 z_h} \sum_{k=1}^{h-1} e^{\alpha(z_k - z_h)} = T_1 - j\frac{k_0}{4\pi b^2 \ln(d/b)} e^{-jk_0 z_h}.$$

Thus simply ordering the terms, one gets

$$M_\varphi^{(1)}(z_h) = \alpha_m H_{0\varphi} e^{-jk_0 z_h} \left\{ 1 - j\frac{k_0}{4\pi b^2 \ln(d/b)} \left[\alpha_m + (\alpha_m + \alpha_e) F_h e^{-\alpha z_h} + (\alpha_m - \alpha_e) B_h \right] \right\},$$

where

$$F_k = \sum_{w=1}^{k-1} e^{\alpha z_w} \quad \text{and} \quad B_k = \sum_{w=1}^{N-k} e^{-(j2k_0+\alpha)(z_{w+k}-z_k)} = \sum_{w=1}^{N-k} e^{-j(2k_0+\alpha)\sum_{t=1}^{w} D_{k+t}},$$

with $D_k = z_k - z_{k-1}$ being the distance between two consecutive holes ($k = 1, \ldots, N$). The identity

$$z_{w+h} - z_h = \sum_{w}^{t=1} D_{h+t}$$

is useful to take into account the case of randomly spaced holes, where $D_k = \bar{D} + \delta_k$ with δ_k a random variable.

Appendix B

The relation (42) was first obtained numerically from (41), having chosen practical values for the dimensionless parameter $\alpha = D/\sigma$. Here we report an (more elegant) analytical study based on [18] to prove that

$$S = \sum_{h=1}^{N-1} (N-h) e^{-(hD/\sigma)^2} \left[2\left(\frac{D}{\sigma} h\right)^2 - 1 \right] = \frac{1}{2}\left[N - \left(\frac{\sigma}{D}\right)^2 \right]$$

We can rewrite (41) as

$$S = 2\alpha^2 N S_2 - N S_0 - 2\alpha^2 S_3 + S_1 \qquad \text{where} \qquad S_k = \sum_{h=1}^{N-1} h^k e^{-\alpha^2 h^2} \tag{66}$$

and we try to express S_k in terms of proper integrals of

$$f_k(x, \alpha) = x^k e^{-\alpha^2 x^2} \qquad k = 0, \ldots, 3. \tag{67}$$

First of all, let's notice that

$$\frac{\partial f_k}{\partial h}(h, \alpha) = k f_{k-1}(h, \alpha) - 2\alpha^2 f_{k+1}(h, \alpha). \tag{68}$$

The relation between the sum S_k and the integral of f_k is shown in Fig. 10, for an arbitrary function. The dashed area represents the generic term of the sum, provided that $\Delta h = 1$; its difference with the integral is the area of the region ABC. In first approximation, we can consider that region as a triangle of base Δh and height

$$|f(h) - f(h-1)| = \left| \frac{\partial f}{\partial h} \right| \Delta h$$

and its area is shown in the figure. This has to be added or subtracted depending on which lower limit of the integral is chosen; in formulae:

$$\sum_{h=1}^{N-1} h^k e^{-\alpha^2 h^2} = \int_0^{N-1} f_k(x,\alpha)dx + \frac{1}{2}\sum_{h=1}^{N-1}\frac{\partial f_k}{\partial h}(h,\alpha)$$
$$= \int_1^{N-1} f_k(x,\alpha)dx - \frac{1}{2}\sum_{h=1}^{N-1}\frac{\partial f_k}{\partial h}(h,\alpha)\ . \qquad (69)$$

Performing the integration from 0, we have to compare the rectangle of height $f(h)$ and width Δh (dashed area) with the integral from $f(h-1)$ to $f(h)$; on the contrary, that rectangle will be compared with the integral from $f(h)$ to $f(h+1)$ if the integration itself starts from 1. Obviously, Fig. 10 deals with the first case. Defining

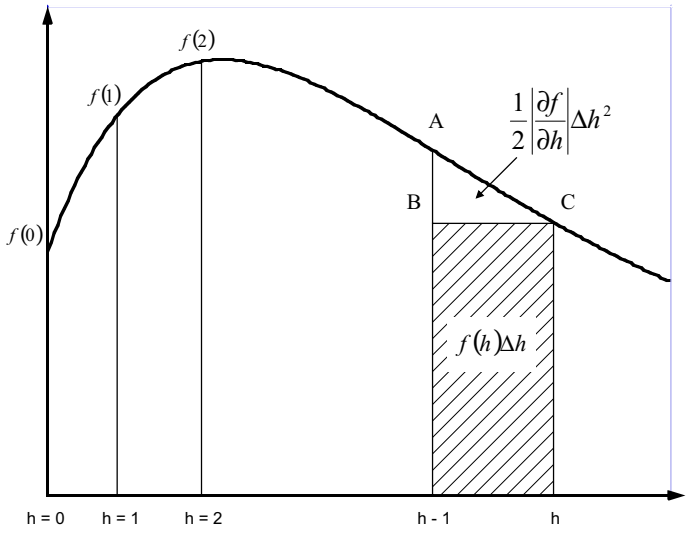

Figure 10: Relation between the sum and the integral. The difference between the dashed area and the integral can be approximated by a triangle, for sufficiently smooth functions.

$$I_k = \int_0^{N-1} f_k(x)dx = \int_0^{N-1} x^k e^{-\alpha^2 x^2} dx$$

and using Eq. (68) in the first one of Eqs. (69) yields

$$S_k = I_k + \frac{k}{2}S_{k-1} - \alpha^2 S_{k+1}. \qquad (70)$$

The preference of the first one of Eqs. (69) is arbitrary; choosing the second one, we would obtain a relation similar to Eq. (70) with a different definition of I_k and opposite signs of the last two terms. The integrals I_k are easily solved in closed form:

$$I_0 = \frac{\sqrt{\pi}}{2\alpha} Erf[(N-1)\alpha] \qquad I_1 = \frac{1-e^{-(N-1)^2\alpha^2}}{2\alpha^2}$$
$$I_2 = \frac{\sqrt{\pi}}{2\alpha} Erf[(N-1)\alpha] - \frac{N-1}{2\alpha^2} e^{-(N-1)^2\alpha^2} \qquad I_3 = \frac{1}{2\alpha^4} - \frac{1+(N-1)^2\alpha^2}{2\alpha^4} e^{-(N-1)^2\alpha^2} \qquad (71)$$

The recursive relation (70) can be used to compute exactly each S_k from the knowledge of I_k; the number of meaningful terms to be taken into account depends on the value of α.

Taking

$$S_0 \simeq I_0 - \alpha^2 I_1, \quad S_1 \simeq I_1, \quad S_2 \simeq I_2, \quad S_3 \simeq I_3 \tag{72}$$

and substituting in Eq. (66), eventually we get:

$$S = \frac{1}{2}\left(N - \frac{1}{\alpha^2}\right) + \left[\frac{1}{2\alpha^2} - \frac{3}{2}N + 1\right] e^{-(N-1)^2\alpha^2}; \tag{73}$$

in the limit of large N the last expression gives Eq. (42). The assumption behind Eq. (72) is somehow arbitrary and it is justified a posteriori comparing Eq. (42) with the exact value (Eq. (41)); however the rigorous derivation from Eq. (70) is not worthwhile since the number of terms to be taken into account depends on how much α is smaller than 1.